



# Methods for improving visibility measurement standards of powered industrial vehicles



Roger Bostelman<sup>a</sup>, Jochen Teizer<sup>b,\*</sup>, Soumitry J. Ray<sup>b</sup>, Mike Agronin<sup>c</sup>, Dominic Albanese<sup>c</sup>

<sup>a</sup> National Institute of Standards and Technology, 100 Bureau Drive, MS 8230, Gaithersburg, MD 20899, United States

<sup>b</sup> Georgia Institute of Technology, 790 Atlantic Dr. N.W., Atlanta, GA 30332-0355, United States

<sup>c</sup> Direct Dimensions Incorporated, Owings Mills, MD, United States

## ARTICLE INFO

### Article history:

Received 21 December 2012

Received in revised form 21 August 2013

Accepted 26 August 2013

Available online 25 September 2013

### Keywords:

Blind spots

Equipment and vehicle operator visibility

Standards and regulations

Sensors and algorithms for measuring

forklift visibility

Pedestrian safety

## ABSTRACT

Poor visibility of powered industrial vehicles, such as forklifts, used in industry is often the cause of accidents that include pedestrians. Current standards allow up to 20% non-visible regions for forklifts where measurement of these regions is performed by using lamps. A collaboration of research organizations, including National Institute of Standards and Technology, Georgia Institute of Technology (NIST), and Direct Dimensions, has been evaluating advanced methods for measuring a forklift operator's visibility. These methods can potentially improve visibility standards. They can also aid forklift and sensor manufacturers to (a) perform different facets blind spot analysis without requiring extensive and time consuming infrastructure set up (b) develop techniques to efficiently utilize visibility-assist sensors and (c) find the optimal location where worker-on-foot or obstacle avoidance proximity detection and avoidance sensors or alerts can be mounted on forklifts. This paper includes explanation of visibility measurement experiments performed and results, associated language suggested to standards organizations, and a prototype design for measuring the visibility of forklifts automatically.

Published by Elsevier Ltd.

## 1. Introduction

Eighty percent of forklift accidents involve pedestrians. Such accidents occur on average of once every three days (Austin et al., 2009). American National Standards Institute/Industrial Truck Standards Development Foundation (ANSI/ITSDF) B56.11.6 “establishes the conditions, procedures, equipment, and acceptability criteria for evaluating visibility of powered industrial trucks.” (ANSI/ITSDF B56.5-2012, 2012) The ANSI/ITSDF B56.5 standard, which references B56.11.6, “defines the safety requirements relating to the elements of design, operation, and maintenance of powered, not mechanically restrained, unmanned automatic guided industrial vehicles and automated functions of manned industrial vehicles.” (ANSI/ITSDF B56.11.6-2005, 2005) B56.11.6 will soon be harmonized with the International Organization for Standardization/Final Draft International Standard (ISO/FDIS) 13564-1 (ISO/FDIS 13564-1-2012, 2012) and therefore, the ISO standard was also used as guidance for this research. The B56.11.6 standard allows up to 20% of the regions surrounding a forklift to be obscured from the operator. Nonetheless, operators are typically declared at fault for the accidents. NIST supports the

development of B56 standards by performing measurements towards improved test methods and serving on the B56.5 standards committee, which includes manned forklifts with automated functions.

The NIST Mobile Autonomous Vehicles for Manufacturing (MAVM) project has been researching forklift safety (Bostelman et al., 2009; Bostelman and Liang, 2011; Bostelman and Shackelford, 2009) because forklift accident rates are continuing to increase. MAVM is investigating the potential for using onboard sensors integrated with semi-autonomous vehicle control to detect obscured regions and improve safety. However, B56.11.6 measurement methods provide only information about how much of the area is not visible to the operator. Advanced operator visibility measurement technology and methods could potentially map obscured regions, as well as suggest sensor mounting locations and the fields-of-view (FOV) needed to maximize the likelihood of detecting obstacles in those regions.

The current ANSI/ITSDF B56.11.6: 2005 standard, soon to be called B56.11.6.1, and the ISO/FDIS 13564-1 (Bostelman and Shackelford, 2009) standard include a test method that uses a row of lights positioned where a forklift operator's head would be and shadows cast by the lights on a test board marked with a grid pattern. The shadows are equivalent to occluded regions and are quantified by counting the grid's blocks. Measurements are referenced to the seat index point (SIP) which is located on a standard apparatus fixed to the seat and considered to be equivalent to the

\* Corresponding author.

E-mail addresses: [roger.bostelman@nist.gov](mailto:roger.bostelman@nist.gov) (R. Bostelman), [teizer@gatech.edu](mailto:teizer@gatech.edu) (J. Teizer), [soumitry@gatech.edu](mailto:soumitry@gatech.edu) (S.J. Ray), [magronin@dirdim.com](mailto:magrnonin@dirdim.com) (M. Agronin), [dalbanese@dirdim.com](mailto:dalbanese@dirdim.com) (D. Albanese).

intersection on the central vertical plane through the seat centerline of the theoretical pivot axis between a human torso and thighs. Fig. 1 shows a test setup on a NIST-owned forklift showing (a) the SIP apparatus and weight bar, (b) the light bar, and resultant shadows from the light bar (c) on a test board as specified in the standard and (d) on a mannequin instead of the test board. That test method shows that there are occluded regions, but does not specify their exact locations. Occlusion is caused by vehicle self-obstructions. Advanced imagers could be mounted to detect obstacles/pedestrians in these occluded regions. The current light method provides only the direction having occluded regions and not the positions on the forklift where sensors might be mounted to compensate for the occlusions.

Several approaches have been developed to measure blind spots of equipment. These approaches can be classified into 2 categories: (a) manual and (b) computer simulation methods. A manual technique, based on the ISO 5353 standard, requires an artificial light source to be mounted at the operator's seat using a Seat Index Point (SIP) apparatus. Visibility of a test body or test screen is then measured following the ISO 13564-1 standard for powered industrial vehicles (Bostelman and Liang, 2011). Such approaches are typically time-consuming and require extensive set-up to measure visibility. As an alternative, the National Institute of Occupational Safety and Health (NIOSH) proposed a "low-tech alternative" (NIOSH, 2012a). This procedure involves preparing a polar grid test bed around the equipment with the operator's seating location at the center of the grid. The visible areas are then marked around the equipment on this polar-grid manually depending on the operator's perception of the grid's visibility. The approach was primarily proposed for construction companies, labor unions, and training organizations to better understand the blind areas around their own equipment. However, this approach is "subjective" as it involves the "human element" in measuring visible regions around equipment.

Computer simulation methods require CAD models of equipment to develop blind area diagrams. Software based artificial lighting is used to determine the blind areas (NIOSH, 2012b; Hefner et al., 2004). The measurements produce blind area diagrams on ground plane, and on planes at 900 mm and 1500 mm vertical distance from the ground. This approach allows measuring direct visibility and indirect visibility (visibility due to mirrors). However, industrial or construction site equipment may undergo modification in which case the blind spots map may change after the equipment has been purchased by a user.

Exact blind spot causes from vehicle hardware and sensor field-of-view (FOV) can provide vehicle manufacturers with more knowledge about how to design a safe vehicle or to retrofit an existing vehicle with safety sensors. Ideally, an automatic system could be designed to measure vehicle blind spots, allow virtual blind spot display, and can provide this knowledge to the operator. NIST and Direct Dimensions, Incorporated (DDI) have been performing measurements of forklifts to develop an automated

visibility measurement system for industrial vehicles using advanced methods (Agronin and Albanese, 2012). The measurement methods include three approaches: (1) use a computer aided design (CAD) model of an industrial vehicle provided by the original vehicle manufacturer and imported into a 3D rendering tool for analysis, (2) laser-scan the vehicle to create a 3D model equivalent to a CAD model, which can be imported into the 3D rendering tool for analysis, or (3) create a panoramic photo from the driver's eye position, process the image, and import it into the modeling software to make the same visibility measurements per the standard.

The RAPIDS Construction Safety and Technology Laboratory at the Georgia Institute of Technology (GT) has also been performing visibility measurements of construction equipment (Teizer et al., 2010). Blind spots on construction equipment result in poor operator visibility and are one of the leading causes of contact collisions in the construction industry. 75% of the struck-by fatalities involve heavy equipment which is primarily due to visibility-related issues (Hinze and Teizer, 2011). Further analysis shows that 55% of the visibility-related fatalities were caused due to equipment blind spots and 57% of the same fatalities were caused due to travel in reverse direction (Hinze and Teizer, 2011). Research at GT has also uncovered new visibility measurement approaches that do not rely on existing equipment CAD models and thus have the potential to solve limitations in reported relevant safety statistics and current standards. GT's visibility measurements and analysis included: data from laser scanning of the vehicle used as input for an automated blind spot measurement tool, a ray-tracing algorithm, grid representation of the vehicle, and the development of an automated blind spot measurement tool. The results show the visibility of personnel on the ground from the vehicle operator's perspective. Fig. 2 shows blind spot results of a dozer when using the GT method.

Typically raw laser scan data of equipment yields millions of points depending upon the resolution of the scan (Teizer et al., 2010). A more recent study by Ray and Teizer (Ray and Teizer, 2013) focused on reducing computational costs incurred due to the size of the laser scan data. This was achieved by computing the blind spots in a spherical coordinate system instead of a Cartesian coordinate system. Owing to the inherent nature of the ray casting algorithm, a significant performance benefit was achieved. The approach was validated on 36 synthetic point clouds for which the ground truth (actual locations) of the blind spots were known a priori. Furthermore, the developed methodology allows computing different facets of blind spot such as: (a) volumetric blind spot, (b) blind spots map, (c) rectangular 1 m boundary visibility, (d) 12 m circumference analysis, and (e) worker visibility analysis.

The DDI approach is explained in this paper, which includes a detailed workflow for each of the three approaches, results from measuring a NIST forklift. Block diagrams show how to automate the visibility measurement analysis using modeling and rendering. This paper also includes an explanation of the new GT analysis approach and results using the DDI collected data of the NIST forklift.

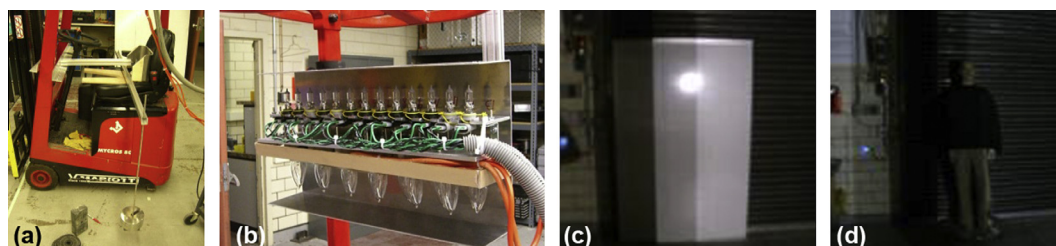
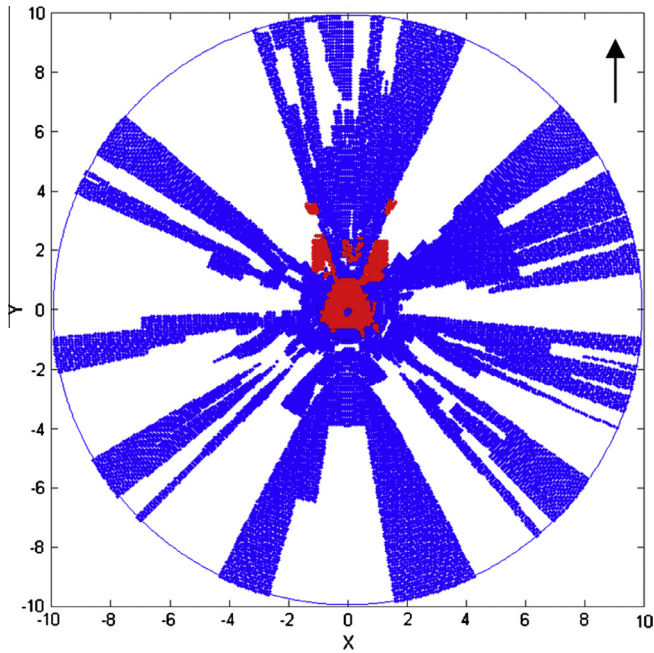


Fig. 1. Test setup on a NIST-owned forklift showing (a) the seat index point (SIP) apparatus and weight bar, (b) the light bar, and resultant shadows from the light bar (c) on a test board as specified in the standard and (d) on a mannequin instead of the test board.



**Fig. 2.** Plan view of the blind spots (blue areas) of a dozer in a 10 m radius at ground level. (For interpretation of the references to colour in this figure legend, the reader is referred to the web version of this article.)

A comparison of the DDI and GT approaches follows along with suggested standard test method language for potential proposal to the ANSI/ITSDF B56.11.6.1 standard committee.

## 2. Experiments

Operator visibility measurements were performed using a NIST-owned forklift having a 4000 kg capacity and 5 m lift height. Four different approaches were tested and are explained in this section: (1) Using a computer aided design (CAD) model of an industrial vehicle provided by the original vehicle manufacturer and imported into a 3D rendering tool for analysis, (2) Laser-scanning the vehicle to create a 3D model equivalent to a CAD model, which can be imported into the 3D rendering tool for analysis, (3) Importing data created from a panoramic photo taken from the driver's eye position into the modeling software to make the same visibility measurements per the standard, and (4) Using a computational approach on laser scan data of equipment (Ray and Teizer, 2013; Marks et al., 2013; Franaszek et al., 2009). Fig. 3 shows a flow diagram for the first three approaches. All tests were to provide outputs similar to the criteria shown in the ISO/FDIS 13564-1 standard for ride-on forklifts which states:

When traveling the forklift, in all positions along the test path, there shall be one or more illuminated areas for both requirements (a) and (b) of at least the following:

- (a) Forward and rearward directions:
  - 20% of the vertical surface of the test body when illuminated from less than 35° above horizontal, or
  - 100% of the horizontal surface of the test body when illuminated from 35° or more above horizontal;
- (b) Forward direction: at least 20% of any 500 mm × 500 mm surface on the test screen shall be illuminated, not considering the dark shadows cast by the vertical structural members of the mast (channels, I-beams and/or the vertical section of a telescopic boom).

- When maneuvering the forklift, there shall be one or more illuminated areas of at least:
  - 20% of the vertical surface of the test body when illuminated from less than 35° above horizontal, or
  - 100% of the horizontal surface of the test body when illuminated from 35° or more above horizontal.

### 2.1. Visibility measurement via CAD model

It is reasonable to assume that a vehicle manufacturer has a detailed CAD model of each of their vehicles. A CAD model can be used directly to measure visibility rather than to measure the actual vehicle. The approach is summarized in Fig. 3 (left). All subsequent measurement approaches are based on this, unless stated otherwise. Below we present a detailed discussion on each step researchers followed in this approach.

#### 2.1.1. CAD model of vehicle

The CAD model must be a solid model that includes any surface visible from the cabin, plus the seat, mast, and fork tines. A CAD model for the NIST-owned example vehicle was not available, so researchers created a model to develop this test method by using laser scans. The model created is shown in Fig. 4. The CAD model must be configured with the boom and forks in the proper position for measurements to meet the required standards. The current ANSI standard requires the mast to be angled back and the forks to be within a certain height range. The ISO standard, however, requires two mast positions: vertical and angled back.

#### 2.1.2. Vehicle and the SIP dimension measurement

The vehicle and SIP dimension measurements are required to determine the location of the lamps and the projection screens to meet the required standards. Length and width of vehicle can be obtained directly from the CAD model. The SIP dimensions may be known to the manufacturer or may need to be measured using a fixture on an actual vehicle. The SIP should be determined relative to a reference point in the CAD model, such as the floor, left extents of the vehicle, and front face of the vehicle.

#### 2.1.3. CAD model to mesh format

Most CAD packages can export solid models into meshed (polygonal) format, such as .OBJ, .PLY, or WRL. This conversion step is necessary to be able to import the model into image rendering software.<sup>1</sup>

#### 2.1.4. Parametric model of the screen and lamp positions

The image rendering software created a 3D model of each projection screen and each lamp in the lamp array. This model is parametric, meaning that the absolute position of each screen and lamp is a function of the dimensions from step 2.1.2. These positions, and even the number of lamps required, are completely different depending on which visibility standard is used for assessment. However, the parametric model can be designed to accommodate both standards.

#### 2.1.5. Rendering macro

Image rendering software contains a ray-tracing module that can shine virtual light sources through a scene and project the shadows onto a surface. This capability allows users to create a table of lamp positions, orientations, and projection screens that cor-

<sup>1</sup> Certain trade names and company products are mentioned in the text or identified in an illustration in order to adequately specify the experimental procedure and equipment used. In no case does such an identification imply recommendation or endorsement by the National Institute of Standards and Technology, nor does it imply that the products are necessarily the best available for the purpose.

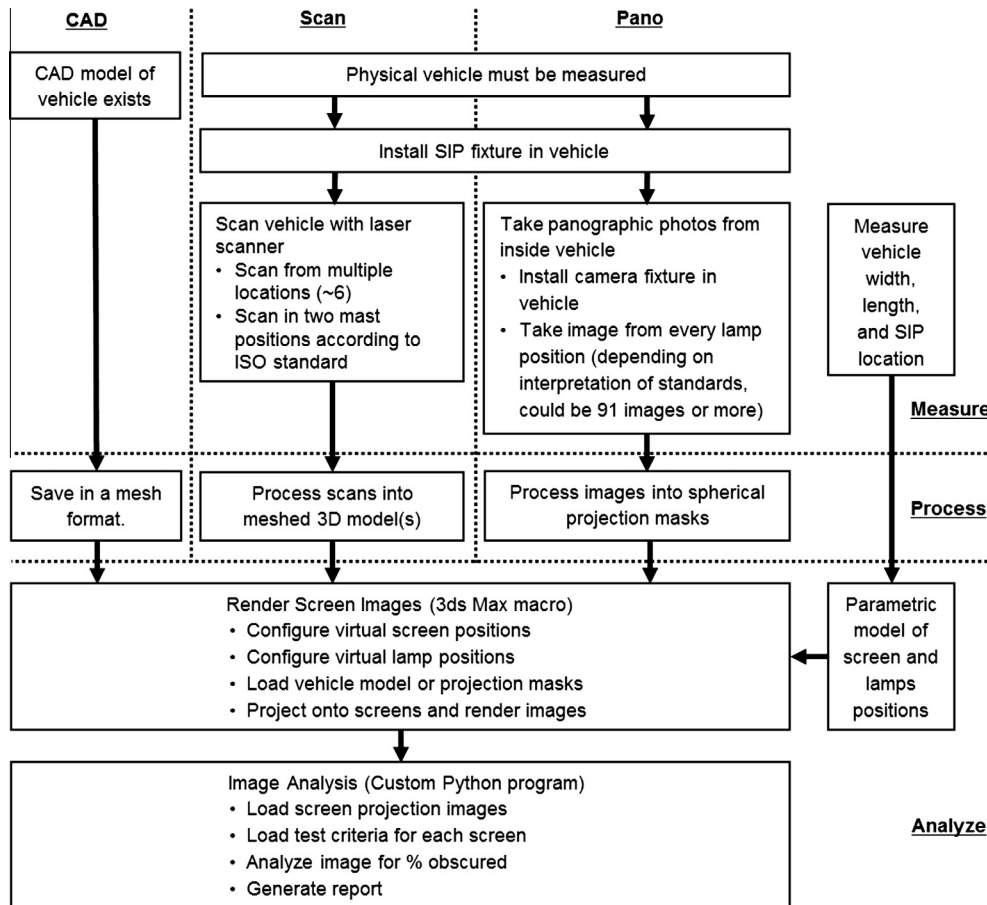


Fig. 3. Approaches to digital measurement of visibility: CAD-model (left), Laser-Scan (middle), and Photo Panograph (right).

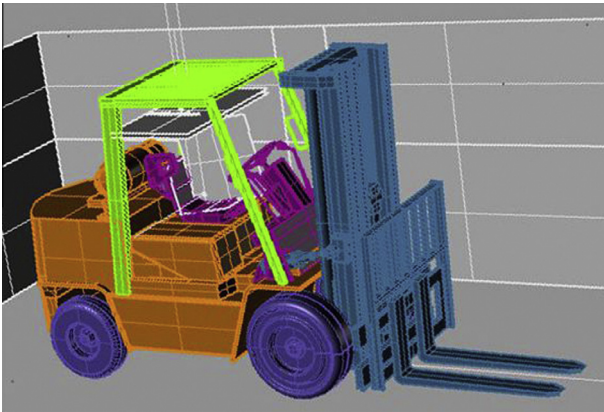


Fig. 4. CAD model of the forklift created from laser scans of the vehicle, rather than from the manufacturer.

respond to each of the tests in the standard. For each lighting configuration, shadows are rendered onto the screen and the screen images are saved. The lamps can be assigned a fixed brightness, so that by measuring the gray-scale of the projected screen, one can determine exactly how many lamps in the array are illuminating a particular spot. Only spots with zero brightness are in full shadow from all the lamps. This makes the technique superior to using actual lamps, where the edge of a shadow may be ambiguous. Fig. 5 shows a screen shot of the virtual lamps (black and yellow triangles) shining through the forklift CAD model onto a virtual screen and Fig. 6 shows a sample image of ANSI/ITSDF B56.11 test

2a, straight ahead and down. Note in Fig. 6 the gray areas that when blocked and not blocked lamps are combined, provide some shadow. Therefore, the virtual lamps that are blocked by vehicle structure can provide additional non-visible viewpoint information than what is currently requested by the standard.

#### 2.1.6. Image analysis and reporting

The final step in the measurement process was to analyze each rendered screen as per the standard. For most of the tests in the ANSI standard, a 500 mm × 500 mm box is moved through every possible position on the screen. The vehicle fails the test if more than 80% of the box area is in shadow. The ISO standard required less than 80% shadow in a 500 mm × 1200 mm area. This step can be automated with a programming language that includes a powerful image analysis library. A program can be developed to analyze the shadowed area of each image according to the standard's requirements. Determining the percentage of black pixels (black pixels denote shadows) within a specified area in an image is relatively easy to implement. Fig. 7 shows the sample image from Fig. 6 with the area with maximum shadow outlined in red.

#### 2.2. Visibility measurement via meshed model of laser scan

If a CAD model of the vehicle is not available or the manufacturer's CAD model does not represent the as-built vehicle, a 3D model in a mesh format created from scan data can be analyzed using the same process as for a CAD model. The process is described in the sections below.

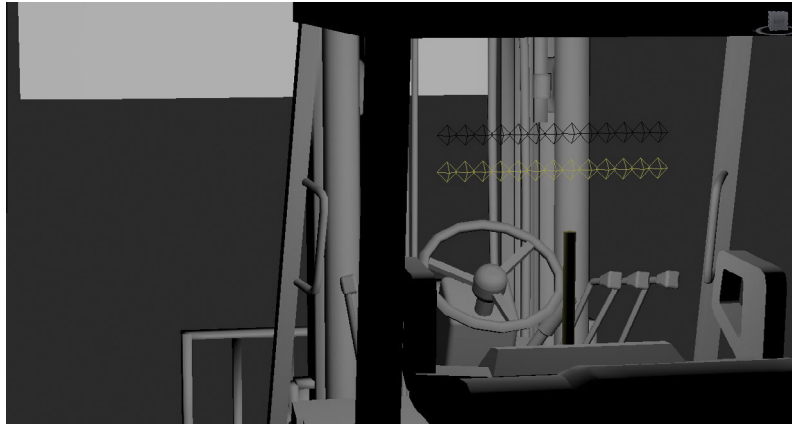


**Fig. 5.** Screen shot of the virtual lamps (black and yellow triangles) shining through the forklift CAD model onto a virtual screen. % (For interpretation of the references to colour in this figure legend, the reader is referred to the web version of this article.)

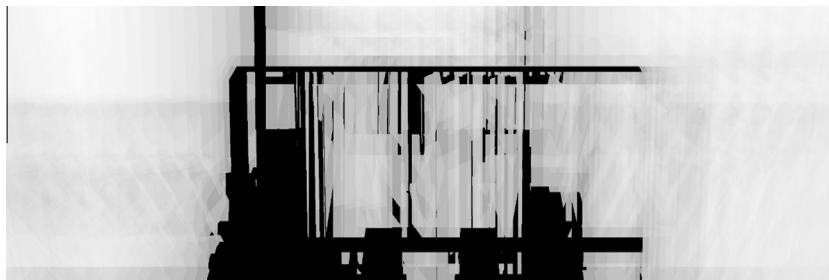


**Fig. 6.** Sample image of ANSI/ITSDF B56.11 test 2a, straight ahead and down.



**Fig. 7.** Sample image from Fig. 6 showing area with maximum shadow.

### 2.2.1. Physical vehicle to be scanned

Laser scanning can capture the geometry of an object with millimeter accuracy and resolution. This is an ideal tool for creating a 3D model of a complex object. This process was demonstrated by scanning a sample vehicle, provided by NIST.

### 2.2.2. SIP fixture installation

A fixture built by NIST to locate the SIP was utilized. The fixture was loaded with a spring scale (lateral load) and weights as per ISO 5353. Fig. 8 shows the NIST-built, SIP fixture in place and loaded with weights, as well as the light bar and resultant images.

### 2.2.3. Scan the vehicle

The sample vehicle was scanned with a spherical laser scanner. It measures with  $\pm 2$  mm accuracy and about 2 mm resolution. Spheres were attached to the vehicle and the surrounding floor to assist with the alignment of scans taken from different points

of view. The scanner was positioned at eleven locations around the outside of the forklift to capture every surface – inside and outside the cabin of the forklift. Additional scans of the forklift were taken with the SIP fixture installed and with the mast in different positions. Fig. 9(a) shows the forklift with reference spheres attached and (b) shows the forklift being scanned in one of eleven scanning positions.

### 2.2.4. Process the scans

A laser scanner is a line-of-sight device where the data from each scan covers only parts of the geometry. Each scan contains several million points of 3D data, in a format called a “point cloud.” To make a complete model from the scans, it is necessary to align or register the overlapping portions of the individual scans. This can be done using software to find a mathematically best fit between the overlapping geometry, or by aligning common reference points, such as the spheres attached to the vehicle. Scene visualiz-



Fig. 8. The NIST-built, SIP fixture in place and loaded with weights.

ing software aligned the scans using both the techniques which delivered satisfactory results. The result was a single point-cloud containing the points from all 11 scans. Although some research has been done in this area (Dimensions, 2012), this registration process is not fully automatable by current off-the-shelf software, but it is not a difficult process to automate. Fig. 10 shows a point cloud of the forklift comprising over 20 million points registered with eleven scans. The data in a point cloud is literally a collection of standalone 3D points. There are no surfaces or solid objects to occlude light in the rendering software so surfaces have to be wrapped around these points.

As part of our exploration of techniques, we initially created a CAD model from the point cloud. This is a difficult process requiring more specialized software. The modeler essentially traces over the point cloud, fitting surfaces to the points. While we would not recommend this process for non-experts, the result for this study was a CAD model that could be configured in many ways (the mast and forks are adjustable), and this allowed us to evaluate our first approach, visibility measurement via CAD model. A simpler technique is to create a mesh model by constructing a series of connected triangles from the point cloud.

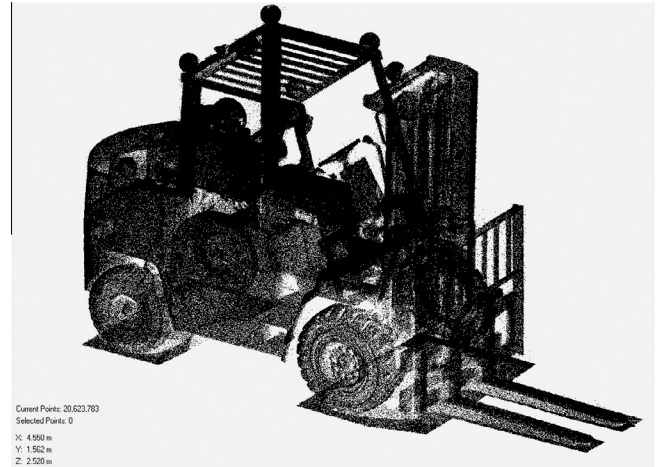


Fig. 10. Point-cloud of the forklift comprised of over 20 million points from eleven aligned scans.

The next step in processing the point cloud into a meshed model is to remove “noise” (points that are not a part of the vehicle) and redundant points to decimate the model in order to reduce memory requirements. Then the mesh can be generated from the remaining points. Mesh processing software was used to delete extraneous points and then create a mesh model. Fig. 11 shows a mesh model of the forklift comprised of about 700,000 triangles.

CAD objects were fitted to the points, resulting in a to-scale CAD model of the forklift. The additional scan data was used to determine the reference surfaces of the SIP fixture and the mast’s axis of rotation. CAD tools were then used to construct the SIP, the locations of the lamps, and the projection screens for visibility measurement.

#### 2.2.5. Measurement of vehicle dimensions and SIP coordinates

A CAD software package was used to measure the length and width of the forklift while creating the mesh model. To determine the SIP coordinates, the CAD software package was used to construct the planes that were fit to the SIP fixture scan data. The SIP was located at the intersection of these planes. While the fixture closely matches the fixture in the standard, the SIP is difficult to locate, since it is measured from the back and bottom surfaces of the fixture which are not accessible when the SIP is weighted down into the driver’s seat. Thus, we had to compensate for the thickness of the fixture. We recommend that the standards committee allow SIP device users to augment the fixture with a sphere, or partial sphere located with its center at the SIP. This will make the SIP much easier to locate relative to other reference surfaces in the vehicle, whether measuring with a tape or a laser scanner, and will

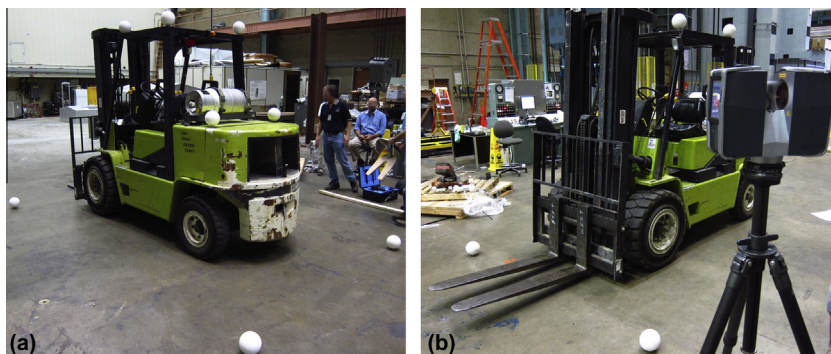


Fig. 9. (a) The forklift with reference spheres attached. (b) Scanning the forklift. One of eleven positions is shown.

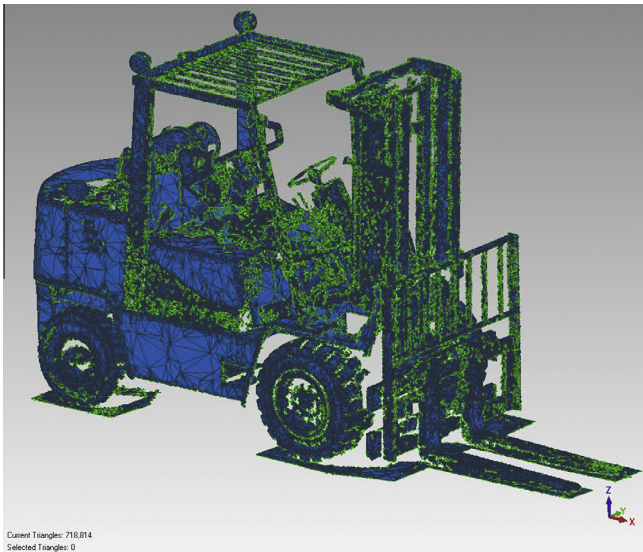


Fig. 11. Mesh model of the forklift comprised of about 700,000 triangles.

not require specialized software to construct the geometry. Fig. 12 shows the SIP location process and planes constructed on the SIP fixture geometry. The actual construction in the CAD software package is difficult to see – thus Fig. 12 was created in a word processing software package on top of the actual point cloud data.

### 2.2.6. Analysis

The remaining steps are the same as for measuring visibility with a CAD model (Sections 2.1.4–2.1.6). The vehicle dimensions and the mesh model are imported into a CAD software package, and the analysis is performed the same way.

### 2.3. Visibility measurement via photo panograph

A novel approach for measuring visibility is to use photo panographs from inside the vehicle. A panograph is a panoramic view created by stitching together a series of overlapping individual images. This is the same technique used to assess pilot visibility in aircraft cockpits. Rather than creating a 3D vehicle model to shadow virtual lamps, we will use a spherical projection from each panograph to mask each virtual lamp, creating the same shadows as the 3D model itself.

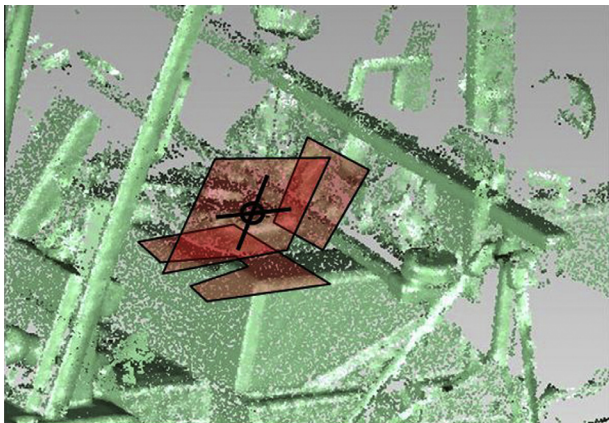


Fig. 12. SIP location process, showing planes constructed on the SIP fixture geometry.

#### 2.3.1. Physical vehicle to be scanned

As with laser scanning, a photo panograph can capture all the geometry seen by the driver from within the vehicle. The panographs do not directly measure the depth. However, the azimuth and elevation angles can be determined with considerable accuracy in the panograph.

#### 2.3.2. Installation of SIP and panograph fixture

The SIP fixture was installed in the same manner as described in Section 2.2.2. Then the panograph assembly was installed. The assembly consists of a standard Red, Green, Blue (RGB) camera and a motorized camera mount. The mount is programmable to automatically move the camera through any number of angles in azimuth and elevation, firing the camera at each position. Fig. 13(a) shows the motorized camera mount, (b) the camera mount clamped to a board over the SIP fixture where a plumb bob hung from the bottom of the clamp was used to center the fixture and adjust the height, (c) a close-up of the camera clamp and plumb bob, and (d) the panograph assembly mounted inside the forklift cabin. Researchers passed a beam through the vehicle cabin and suspended it on two tripods, enabling beam height adjustment. The beam was oriented perpendicular to the vehicle centerline to act as a visual reference for that axis. The motorized camera mount was clamped to the beam at multiple positions to match the position of each lamp in the upper row of the lamp assembly. While this arrangement was sufficient for the forward-facing lamp orientation, another fixture was developed to locate the camera at positions matching the lamp array when it is aimed to the sides or behind the vehicle. Fig. 14 shows a diagram of locating the panographic camera assembly relative to the SIP. Dimensions are taken from the ANSI visibility standard.

To recreate the ANSI test standard, it is necessary to position the panograph at each lamp location in the lamp array (26 positions), with the array in every required configuration (seven angles), for a total of 182 panographs. Since the objective was to demonstrate the process and not take complete data, panographs were taken corresponding to only one row of lamps in the forward-aiming orientation. However, seat bolsters obstructed the camera assembly for the outer-most lamp positions. Thus only eleven panographs were taken, along with one additional panograph, at the center position, with the mast tilted back and the forks raised 1.1 m, to create a worst-case obstruction for the driver.

Because of the difficulty determining the exact location of the SIP, the laser-scan data of the panograph setup was used to determine the exact camera position relative to the SIP. It was observed from the laser scan data to be located at 577 mm above the SIP, which is slightly below the plane of the lower row of lamps.

#### 2.3.3. Vehicle dimension and SIP location measurement

One advantage of measuring visibility via panograph is that an expensive laser scanner is not required. However, the vehicle length and width, and the location of the SIP need to be measured using a tape measure or other less sophisticated alternatives.

#### 2.3.4. Panographic images

The motorized camera mount was programmed to take 16 images around 360° of azimuth, at two different elevation angles. Successive images need to overlap by about 30% in order to stitch well. The elevation angles were set to cover the floor-to-max height of a projection screen at the minimum distance (about 2.2 m above the floor at 1.2 m from the side of the vehicle.) As described above, this sequence of images was taken at eleven positions, and then the 12th panograph was taken from the center position with the forks raised to occlude more of the view.

Another option for taking panoramic photos is to use a spherical, solid-state camera that captures a full panorama with no

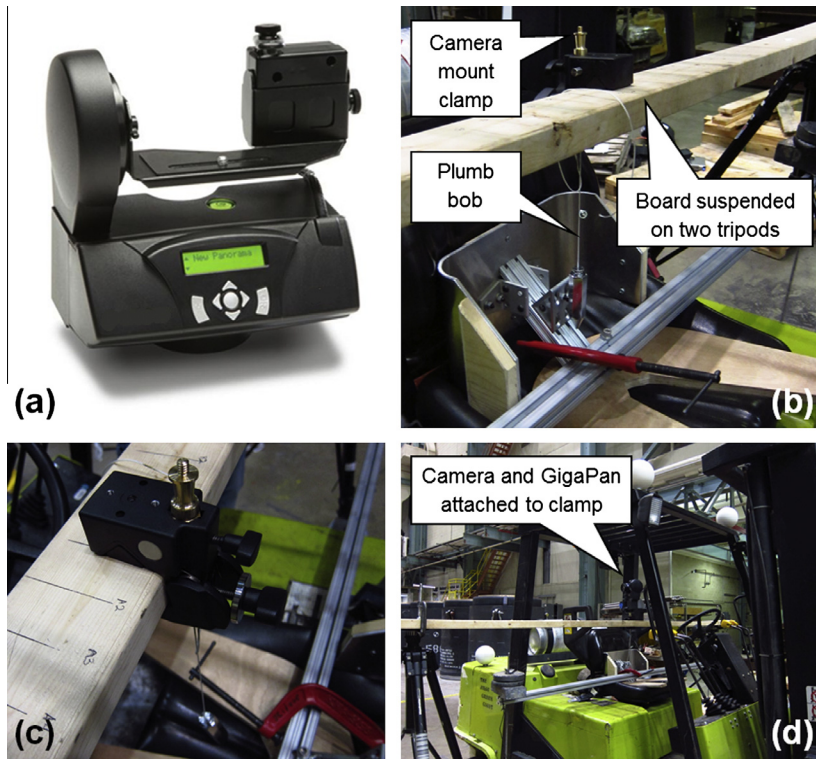


**Fig. 13.** (a) The GigaPan Epic motorized camera mount, (b) the camera mount clamped to a board over the SIP fixture where a plumb bob hung from the bottom of the clamp was used to center the fixture and adjust the height, (c) a close-up of the camera clamp and plumb bob, and (d) the panograph assembly mounted inside forklift cabin.

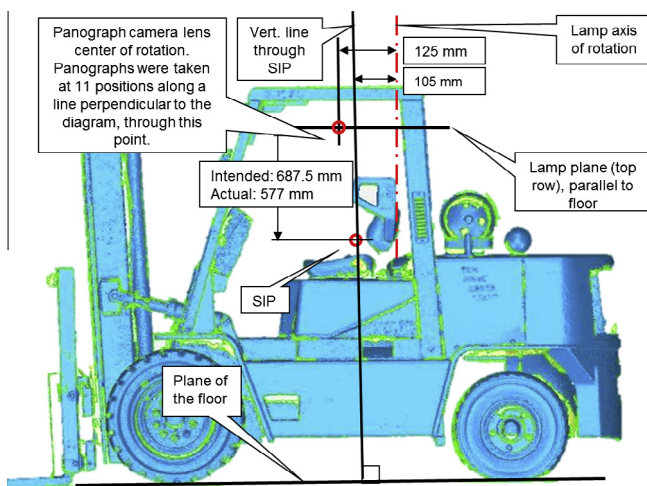


**Fig. 14.** Diagram of locating the panographic camera assembly relative to the SIP. Dimensions are taken from the ANSI visibility standard.

moving parts and thus no image processing is required to stitch the photographs together. This device is potentially more expensive than a standard camera and motorized mount, but it provides a more accurate end result and requires less processing.

### 2.3.5. Process the images into masks

The first step in processing the photos was to stitch all the photographs together into a continuous panorama. This is an automatic process that can be accomplished with several software packages currently available. This software finds common points in adjacent images, and taking the camera's optics into account, automatically stitches the photos together into a panorama in a

spherical space. Vertical pixel position maps to an elevation angle, and horizontal pixel count maps to an azimuth angle in the spherical projection. The only manual step in the process is to indicate  $0^\circ$  azimuth. The support beam was taken as  $\pm 90^\circ$  azimuth reference, and measured to  $0^\circ$ .

The next step was to convert each stitched panograph into masks for the 3D analysis software. We used an open-source photo editor to create a new layer over each image, and then manually traced the contours of the forklift, filling it in with black. This was a manual and tedious process. If it had been possible to take the photographs in a room with a plainer, lighter-colored background, it would have been possible to automate this process by converting the image to two colors (black and white) and adjusting the threshold such that all lighter background pixels turned white. Fig. 15 shows a spherical projection of a panographic view from the driver's eye position and Fig. 16 shows a black and white mask of the same panographic image, centered and expanded to  $360^\circ$  azimuth by  $180^\circ$  elevation. The pixel coordinates correspond exactly to the vector from the eye position in polar coordinates.

### 2.3.6. Load vehicle dimensions into parametric model of lamps and screens

This process is identical to the process described in Section 2.1.4.

### 2.3.7. Macro in 3ds max

Unlike using a CAD or laser-scanned 3D model to shade the lamps, we can import each panograph as a mask that surrounds each virtual lamp. The mask shades the light exactly as if an actual vehicle were in the way. Fig. 17 shows a screen shot of a spherical mask surrounding a virtual lamp.

### 2.3.8. Custom image analysis and report

This process is the same as described in Section 2.1.6.



Fig. 15. Spherical projection of a panoramic view from the driver's eye position.

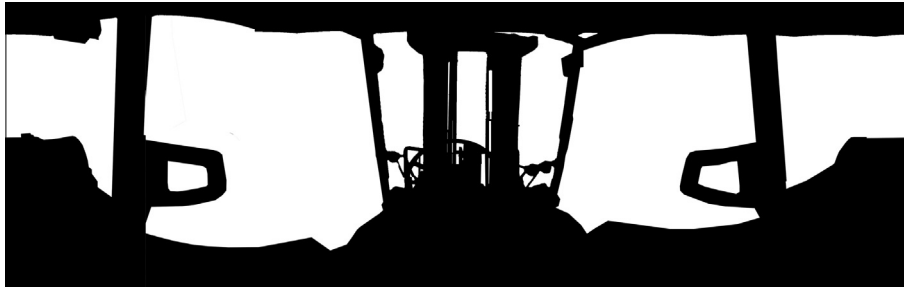


Fig. 16. Black and white mask of the same panoramic image, centered and expanded to 360° azimuth by 180° elevation. The pixel coordinates correspond exactly to the vector from the eye position in polar coordinates.



Fig. 17. Screen shot of a spherical mask surrounding a virtual lamp.

#### 2.4. Visibility measurement via volumetric model of laser scan (Teizer et al., 2010; Ray and Teizer, 2013)

The data input was a laser scan of the forklift. The scan consisted of roughly  $20 \times 10^6$  points. The side and top views of the raw point cloud are shown in Fig. 18(a) and (b), respectively. The point cloud was binned (meaning: represented by a histogram or in simpler terms, a series of buckets) into a three dimensional grid in a spherical coordinate system in steps of size  $\Delta r = 0.05$  m,  $\Delta \theta = 0.3^\circ$ , and  $\Delta \phi = 0.3^\circ$ . The numbers of bins along the three directions were: 416 along  $r$ , 1200 along  $\phi$ , and 600 along  $\theta$ . The number of bins is computed from the step-size values input by the user. Due to memory constraints for storing the three dimensional grid, the step sizes were set to the above minimal possible values.

##### 2.4.1. Volumetric blind spot

Percentage volumetric blind spot in this research is defined as the ratio of total blind area on the surface of a 12 m radius sphere to

the total area of the same sphere lying above the ground plane. The sphere is assumed to be centered at the origin or the head of the operator. The surface of the sphere lying above the ground plane is only considered during the computation. For the forklift shown in Fig. 18, the volumetric blind spot is illustrated graphically in Figs. 19(a) and (b) which show the visible and blind areas on a 12 m sphere centered at the origin. The percentage volumetric blind spot was 19.48%. The time taken for computing the volumetric blind spot was 1.19 s. The visible areas are shown in green; the blind areas are shown in red.

##### 2.4.2. Analysis of blind spots map, 12 m circumference visibility, and rectangular 1 m boundary

**2.4.2.1. Blind spots map.** A blind spots map is the mapping of visible and blind areas contained in a 12 m radius circle lying on the ground plane, with the operator position at the center. For the forklift shown in Fig. 18, the percentage blind spot was computed to be 21.20%. The time taken for computation was measured to be 0.83 s (includes computation of blind spots map, 12 m circumference visibility, and rectangular 1 m boundary analysis).

Table 1 shows the detailed results of the analysis. The circle was divided into four regions: front, right, rear, and left as shown in Fig. 18(b) and the blind spot area in these four regions are shown in Table 1 (bottom four rows). Fig. 20 shows the blind and visible areas contained in the 12 m radius circle lying on the ground plane.

**2.4.2.2. 12 m Circumference visibility.** The 12 m circumference visibility measurement is similar to blind spot map measurement as discussed above; however, here visibility is measured only along the edge of the circle and all measurements are in terms of length. The total length of the circumference ( $2\pi r$ ,  $r = 12.0$  m) was computed to be 75.40 m and the visible length along the circumference was 62.71 m (83.17%). Additionally, the software reports the arcs along the circumference that are invisible as shown in Table 2. Fig. 21 is an annotated graphical representation of the arcs in Table 2.

**2.4.2.3. Rectangular 1 m boundary visibility.** Visibility was measured on the circumference of a rectangular 1 m boundary around the

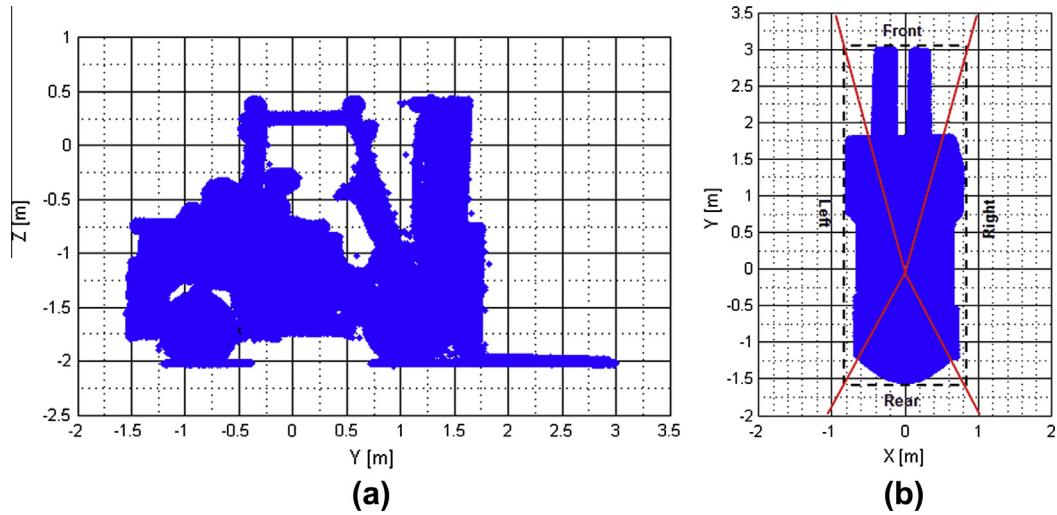


Fig. 18. (a) Point cloud of forklift obtained from laser scan (elevation view) and (b) categorization of area surrounding the equipment into: front, left, right and rear (plan view).

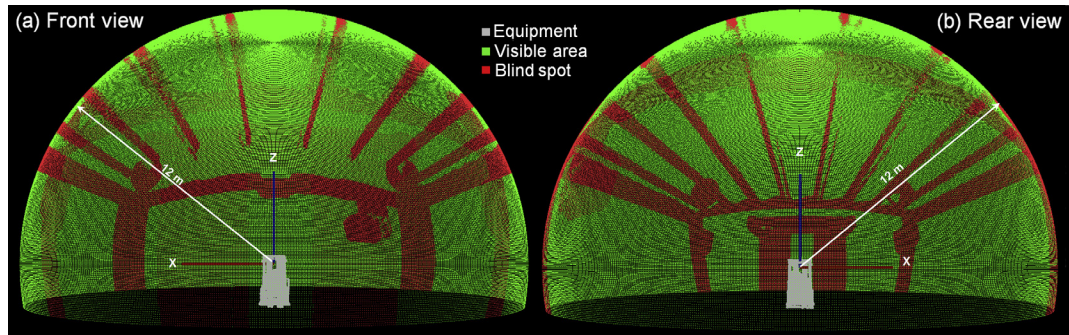


Fig. 19. Volumetric blind spots on a 12 m radius sphere in front (a) and rear (b) view. The red areas represent blind spot regions and the visible areas are represented by green color. (For interpretation of the references to colour in this figure legend, the reader is referred to the web version of this article.)

Table 1  
Blind spot map measurement.

Entity	Area (m <sup>2</sup> )	Percentage (%)
Total area <sup>a</sup>	456.86	100
Blind spot area	96.71	21.20
Visible area	360.15	78.83
Front blind spot	27.08	5.93
Right blind spot	28.90	6.33
Rear blind spot	7.13	1.56
Left blind spot	33.76	7.39

<sup>a</sup> Total area is computed by subtracting the machine footprint area ( $M_{\text{footprint}}$ ) from the circular area ( $C_{\text{areaComputed}}$ ) of 12 m radius.  $M_{\text{footprint}} = \text{Machine width} \times \text{Machine length} = 4.56 \times 1.6 = 7.30 \text{ m}^2$ ,  $C_{\text{areaComputed}} = 463.99.940 \text{ m}^2$ . Thus,  $\text{Total area} = C_{\text{areaComputed}} - M_{\text{footprint}} = 456.69 \approx 456.86 \text{ m}^2$ .

machine. A rectangular 1 m boundary is constructed at an offset distance of 1 m from the smallest rectangle that can be placed around the vertical projection of the machine on the test floor (ground level) on which the machine is located. Table 3 below shows the actual and computed length of this rectangular boundary. The actual length is the calculated perimeter of the rectangular 1 m boundary using the forklift’s dimensions, whereas the computed value is the perimeter calculated by the software in the discretized 3D space. The discrepancy in value arises from the fact that the three-dimensional space is discretized. The visible length was computed to be 9.66 m which constituted 46.78% of the length

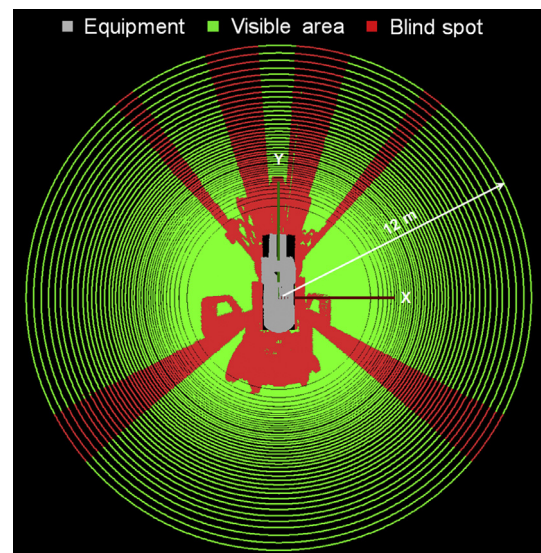
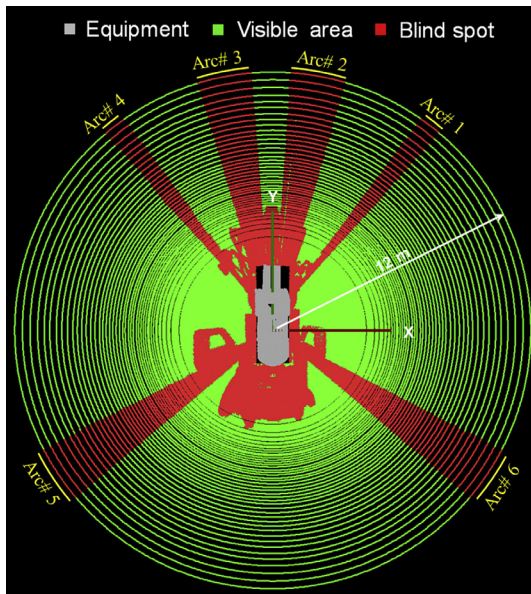


Fig. 20. Graphical representation of blind spot map of the forklift inside a 12 m radius circle.

of the rectangular 1 m boundary. Fig. 22 is a graphical illustration of the visibility along the rectangular 1 m boundary.

**Table 2**  
Invisible arcs along the circumference of 12 m radius circle.

Arc#	From (°)	To (°)	Arc length (m)	Arc angle (m)
1	50.10	55.20	1.07	5.10
2	73.80	86.10	2.58	12.30
3	94.80	107.10	2.58	12.30
4	125.40	130.50	1.07	5.10
5	207.60	220.50	2.70	12.90
6	319.80	332.70	2.70	12.90



**Fig. 21.** Graphical illustration of 12 m circumference visibility.

**Table 3**  
Visibility along the rectangular 1 m boundary.

Entity	Length (m)	Percentage (%)
Total (actual)	20.32	–
Total (computed)	20.65	100
Visible	9.66	46.78
Front blind spot	2.54	12.28
Right blind spot	2.32	11.21
Rear blind spot	2.59	12.54
Left blind spot	3.55	17.20

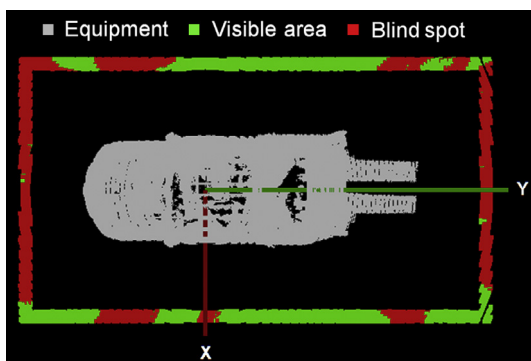


**Fig. 22.** Graphical illustration of visibility along the rectangular 1 m boundary of the forklift.

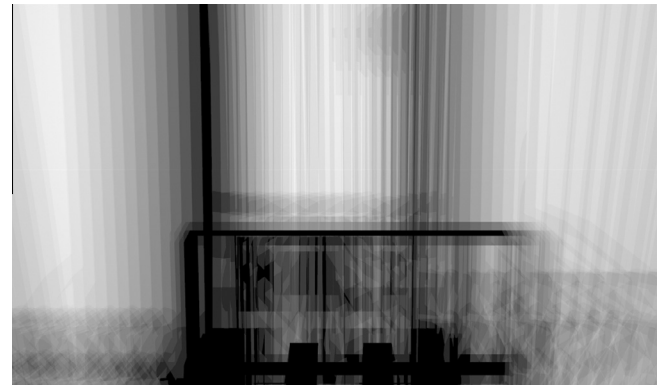


**Fig. 23.** Screen projections 2A (top) and 2B (bottom) (straight ahead) made with the CAD model.

### 3. Results

The DDI measurement results are explained below by comparing methods – CAD Model versus Meshed Model and CAD model versus panographs.

#### 3.1. CAD model vs meshed model

The meshed model from the laser scan produces nearly the same shadow projection as the CAD model, as long as care is taken in processing the meshed model to ensure that no actual obstructions are deleted. Figs. 23 and 24 show screen projections 2A and 2B (straight ahead) made with the CAD model and mesh model, respectively.

#### 3.2. CAD model vs. panographs

The panograph approach can generate results matching the CAD model approach if all conditions are the same. As discussed earlier, the panographs were taken from a position slightly below that required by the standard. However, in the images presented here, the same lighting positions and number of lights for the CAD model and the panographs are recreated. These images are created with one row of 11 lamps. Figs. 25 and 26 show screen projections 2A and 2B (straight ahead) made with 11 lamps positioned inside the CAD model and inside the panograph, respectively.

#### 3.3. Advantages of virtual projections

There are two significant advantages to the virtual projection techniques proposed. First, since ray tracing was used with no diffraction and ideal lamp brightness, there was no ambiguity about the location of shadows. And second, it is possible to get an exact count of shaded pixels for any area in the image, thus making it possible to automate the determination of percent shaded area. Figs. 27 and 28 show how this process can work. Fig. 27 shows projection 2A in gray-scale. Fig. 28 shows the same image converted to black and white. All gray levels have been converted to white. The remaining black areas are total shade. Fig. 29 shows a 500 mm × 1200 mm section of the image in Fig. 27. Gnu Image Manipulation Program (GIMP) analysis software indicates that 42% of the pixels are black, well under the 80% visibility requirement.

#### 3.4. Advantages of laser scanning approach

The primary advantage of this approach is it aids in visualizing different facets of blind spots (see Figs. 19–22), which may other-

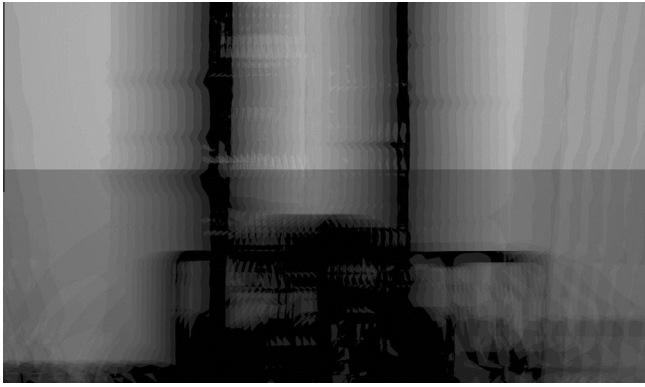


**Fig. 24.** Screen projections 2A (top) and 2B (bottom) (straight ahead) made with the meshed model.

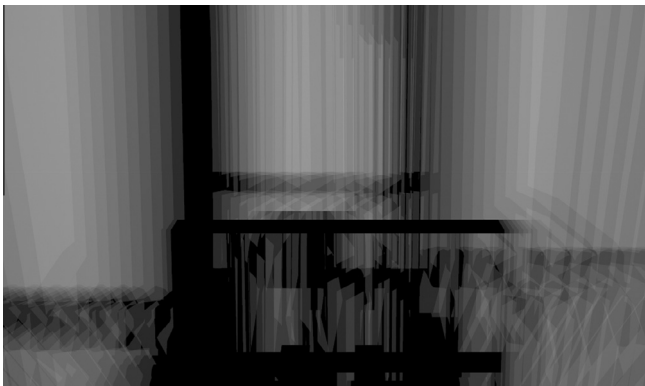


**Fig. 25.** Screen projections 2A (top) and 2B (bottom) (straight ahead) made with 11 lamps positioned inside the CAD model.

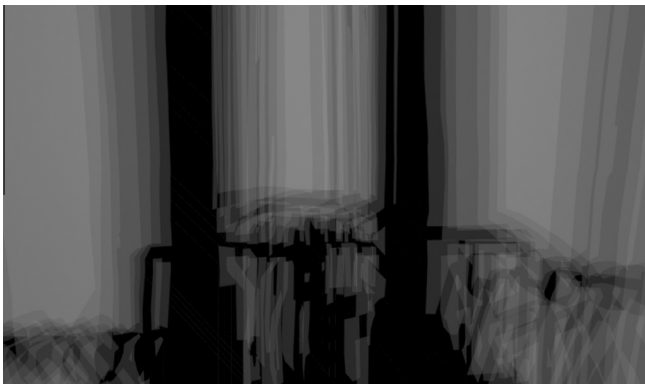


**Fig. 26.** Screen projections 2A (top) and 2B (bottom) (straight ahead) made with 11 panographs.

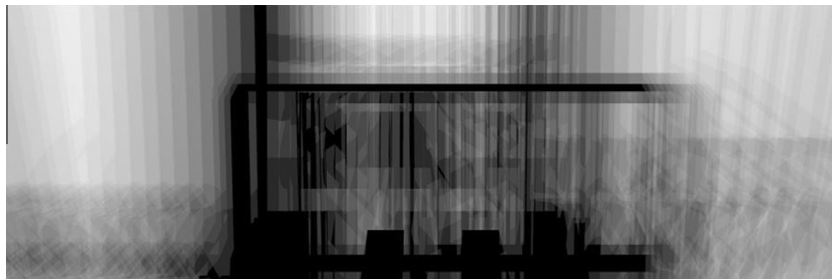


**Fig. 27.** Projection 2A in gray-scale.



**Fig. 28.** The same image converted to black and white. All gray levels have been converted to white. The remaining black areas are total shade.

wise require extensive manual and time-consuming setup. Additionally, since computations are performed in a discretized three-dimensional space, sub-millimeter accuracy in point cloud data is not necessary. Thus, there exists the opportunity to utilize point cloud data generated from other less expensive sources such as range-cameras. Accuracy of computations can be increased further by reducing the discretization parameters of the three-dimensional space. Finally, “objective” measurements provide an avenue to evaluate the designs of vehicle from different manufacturers (Teizer et al., 2010; Ray and Teizer, 2013).

### 3.5. Comparison of measurement techniques: cost and complexity

Given that accuracy is acceptable for all four techniques, Table 4 compares the cost and complexity of implementing each.

### 3.6. Recommendations

Upon initial findings, NIST proposed language to ANSI/ITSDF B56.11.6 including a new Clause 6 Other Test Methods. The two proposed sub-clauses are shown here:

### 3.7. Recording technologies

Other test methods which use recording technologies such as light recording or cameras and halogen lamps or alternate light sources such as light emitting diodes or lasers may be used to conduct the test provided these methods duplicate the standard test procedures in clauses 4 and 5 and produce the same results as the light method,

### 3.8. 3D imaging technologies

Other test methods which use 3D imaging technologies (such as laser scanners), computer modeling, and virtual test objects may be used to conduct the test provided these methods duplicate



**Fig. 29.** 500 mm × 1200 mm section of the image in Fig. 27. GIMP image analysis software indicates that 42% of the pixels are black, well under the 80% visibility requirement.

the standard test procedures in clauses 4 and 5, where the 3D imaging systems replace the halogen lamps, and produce the same results as the light method.

The two sub-clauses provide generic test methods that could utilize the DDI and/or GT methods. However, the sub-clauses do not propose that the DDI and GT methods must be used – thus allowing new methods that provide similar outcome to be used.

If a CAD model of the vehicle is available, and acceptable for use by the standards body, measuring visibility from the CAD model is the most desirable option. This approach has the following benefits.

- Inexpensive to perform.
- Can be completely automated.
- The manufacturer can assess visibility early in the design phase and make changes if desired.

**Table 4**  
Comparing the cost and complexity of implementing the measurement techniques.

Data source	Existing CAD model	Meshed model of laser scan	Panographs from inside vehicle	Volume model of laser scan (Ray and Teizer, 2013)	
Measurement	Cost	• No additional cost	• \$40–\$100 K	• ~\$11 K	
	Complexity	• Use CAD to measure vehicle dimensions • Physical measurement may be required to find SIP coordinates	• Several scans required • Workflow can be standardized	• Accurate positioning of camera at 182 positions for the ANSI standard is required	• Range camera (\$100) • Laser scanners (\$30 K–\$90 K) • Automatic
Processing	Cost	• No additional cost if CAD program can export to mesh format	• Scan alignment software may be included with scanner. Additional point cloud decimation and meshing software ranges from open source but complex to expensive but easy	• Open source image stitching and processing software available	• No additional cost
	Complexity	• Automatic	• Automatable depending on the software • Additional knowledge and skill may be required	• Image stitching is automatic • Generation of black and white mask is manual and tedious (could be automated) • Additionally, large number of photographs to process	• Automatic
Analysis	Cost	• Analysis software is required, plus cost to develop macro and image processing program			• No additional cost
	Complexity	• Processes could be completely automated with custom software			• Automatic

- What-if scenarios can be assessed, incorporating different mast and fork positions, and different load conditions.

If a physical vehicle must be measured, scanning and modeling it with a laser scanner to create a 3D model is the next-preferred option. Although the cost of the laser scanner can be significant, the results of this method can be considerably more accurate and verifiable as compared to using a lamp array and actual projection screens.

The panoramic measurement approach has great promise, but it is not practical for exactly reproducing the current lamp-based method. The problem is that in order to replicate either the ANSI or the ISO standard, measurements need to be taken at an impractical number of positions.

On the other hand, the panoramic technique is used to assess visibility in aircraft cockpits (Dimensions, 2012). If the number of required images could be reduced to under a dozen, this technique could be the simplest and most cost-effective of all. The driver's head can only be in one position at a time. A single panorama provided much more insight into the size and location of blind spots than the current standards. It would also enable the relative comparison of visibility between different vehicle models.

Therefore, a proposed simplified visibility measurement method consists of:

1. A single panorama from the center eye position.
2. Making a black and white spherical obscuration plot.
3. Scanning the plot using a mask with a fixed FOV – This would be similar in intent to scanning the projection screens with a 500 mm × 500 mm box, but would be more physiologically correct since the window could match the FOV of the human macula, the area of most detailed vision, and this FOV would be fixed in every direction, rather than varying with direction.

#### 4. Conclusions

Forklift operator visibility was measured using advanced methods and the current ANSI and ISO standards. We performed a direct comparison of methods to create a basis for determining where visibility sensors could mount on the forklift to assist the operator. Two approaches to creating a mask of the vehicle geometry were

demonstrated: (1) using a 3D laser scanner external to the vehicle and (2) using a panoramic camera inside the vehicle at locations specified by the standards. The two measurement methods captured the vehicle geometry and then a model was created from the scan data equivalent to a CAD model.

Results from the visibility measurement experiments demonstrated that if vehicle measurement is required, scanning the vehicle using a 3D laser and producing a CAD model provided the clearest comparison of visible and non-visible regions. It also provided the easiest method tested towards design of an automated visibility measurement system. Laser scan measurements based on approach (Teizer et al., 2010) provides objective results and visualization of different facets' blind spots. The computations are performed in discretized three-dimensional space. Thus, sub-millimeter accuracy in input data may not be necessary. Other less expensive alternatives might focus in the future on using stereo cameras or range sensors. Latter sensors may be used to develop coarse point clouds as they typically have lower resolution and range compared to commercially-available laser scanners. Feasibility studies and experimental verifications are thus required if researchers or developers proceed in this direction. Presently, laser scanning system cost is higher than the panoramic camera method, which also demonstrated good results. Recommendations included a clause proposed to be added to current standards allowing the use of these advanced measurement methods. Other recommendations were posed that, if the standard allowed a single measurement from a typical operator viewpoint, the panoramic method may provide the most cost effective and simplest method to perform.

Fig. 30 shows the CAD model produced from scanning and the concept of using the model to show where 3D imaging sensors could be mounted to capture non-visible regions. The 3D imaging sensor field-of-views could be provided to sensor manufacturers to produce the necessary sensors for each vehicle type.

The proposed approaches have the potential not only to measure blind spots but also aid in evaluating sensor mounting locations. Additionally, integration of active sensors such as camera systems, ultrasonic sensors, or lasers with the proposed approaches can augment the visibility of the operator in real-time and thus remains an area to investigate in the future. In particular in the area of intelligent Advanced Driver Assistance System (ADAS) numerous approaches have been developed in this regard. Future research and development might also focus on integrating operator head pose (Ray and Teizer, 2012) and eye tracking (Eye-tracking, 2013), worker posture (Ray and Teizer, 2012; Cheng et al., 2013), real-time location tracking of resources surrounding

the vehicle (Cheng and Teizer, 2013a), real-time data visualization (Cheng and Teizer, 2013b), and real-time warning and alert technologies (Pratt et al., 2001; Teizer et al., 2010; Marks and Teizer, 2012) to design and operate intelligent and safe worksites.

## References

- Agronin, M., Albanese, D., 2012. Report to NIST: Visibility Measurement of a Forklift, Solicitation Number SB1341-12-RQ-0222 (August).
- ANSI/ITSDF B56.11.6-2005, 2005. Evaluation of Visibility from Powered Industrial Trucks.
- ANSI/ITSDF B56.5-2012, 2012. Safety Standard for Driverless, Automatic Guided Industrial Vehicles and Automated Functions of Manned Industrial Vehicles.
- Austin, M., 2009. Fork Lift Awareness, Presentation by Occupational Safety and Health Administration, Baltimore/Washington Office, 2009 Performance Metrics for Intelligent Systems Workshop (PerMIS '09), NIST Special Session, September 2009.
- Bostelman, R., Liang, Li P., 2011. Measurement and Evaluation of Visibility Experiments for Powered Industrial Vehicles, NIST Internal, Report #7837.
- Bostelman, R., Lang, Li P., 2011. Measurement and Evaluation of Visibility Experiments for Powered Industrial Vehicles, National Institute of Standards and Technology, NIST Interagency/Internal Report (NISTIR) – 7837 (December).
- Bostelman, R., Shackelford, W., 2009. Performance measurements towards improved manufacturing vehicle safety. In: Proc. 2009 Performance Metrics for Intelligent Systems Workshop (PerMIS), NIST Special Pub. 1112.
- Bostelman, R., 2009. White Paper: Towards Improved Forklift Safety, Pro. 2009 Performance Metrics for Intelligent Systems Workshop (PerMIS), NIST Special, Publication 1112 (September).
- Cheng, T., Teizer, J., 2013a. Modeling tower crane operator visibility to minimize the risk of limited situational awareness. *ASCE Journal of Computing in Civil Engineering*. [http://dx.doi.org/10.1061/\(ASCE\)CP.1943-5487.0000282](http://dx.doi.org/10.1061/(ASCE)CP.1943-5487.0000282).
- Cheng, T., Teizer, J., 2013b. Real-time resource location data collection and visualization technology for construction safety and activity monitoring applications. *Automation in Construction* 23, 3–15.
- Cheng, T., Migliaccio, G.C., Teizer, J., Gatti, U.C., 2013. Data fusion of real-time location sensing (RTLS) and physiological status monitoring (PSM) for ergonomics analysis of construction workers. *ASCE Journal of Computing in Civil Engineering*. [http://dx.doi.org/10.1061/\(ASCE\)CP.1943-5487.0000222](http://dx.doi.org/10.1061/(ASCE)CP.1943-5487.0000222).
- Direct Dimensions, Inc., 2012. Cockpit Simulation. <[http://www.directdimensions.com/port\\_projects.htm](http://www.directdimensions.com/port_projects.htm)> (accessed 11.07.12).
- Eyetracking, 2013. <<http://www.smarteye.se>> (accessed 20.08.13).
- Franaszek, C., Cheok, G., Witzgall, C., 2009. Fast automatic registration of range image from 3D imaging systems using sphere targets. *Automation in Construction* 18, 265–274.
- Hefner, R., 2004. Construction Vehicle and Equipment Blind Area Diagrams. National Institute for Occupational Safety and Health, Report No. 200-2002-00563. <<http://origin.cdc.gov/niosh/topics/highwayworkzones/BAD/pdfs/catreport2.pdf>> (accessed 11.05.08).
- Hinze, J.W., Teizer, J., 2011. Visibility-related fatalities related to construction equipment. *Journal of Safety Science* 49 (5), 709–718.
- ISO/FDIS 13564-1-2012, 2012. (Final Draft International Standard) Powered Industrial Trucks – Test Methods for Verification of Visibility – Part 1: Sit-on and Stand-on Operator Trucks Up to and Including 10 t Capacity.
- Marks, E., Teizer, J., 2012. Safety first: real-time proactive equipment operator and ground worker warning and alert system in steel manufacturing. *Iron & Steel Technology*, AIST 9 (10), 56–69.
- Marks, E., Cheng, T., Teizer, J., 2013. Laser scanning for safe equipment design that increases operator visibility by measuring blind spots. *ASCE Journal of Construction Engineering and Management*. [http://dx.doi.org/10.1061/\(ASCE\)CO.1943-7862.0000690](http://dx.doi.org/10.1061/(ASCE)CO.1943-7862.0000690).
- NIOSH, 2012. Highway Work Zone Safety, Construction Equipment Visibility – Manual Method. <<http://www.cdc.gov/niosh/topics/highwayworkzones/BAD/manualmethod.html>> (accessed 20.07.12).
- NIOSH, 2012. Highway Work Zone Safety, Construction Equipment Visibility – Computer Simulation. <<http://www.cdc.gov/niosh/topics/highwayworkzones/BAD/compsim.html>> (accessed 20.07.12).
- Pratt, S.G., Fosbroke, D.E., Marsh, S.M., Pratt, S.G., Fosbroke, D.E., Marsh, S.M., 2001. Building Safer Highway Work Zones: Measures to Prevent Worker Injuries from Vehicles and Equipment. Department of Health and Human Services, CDC, NIOSH, pp. 5–6.
- Ray, S.J., Teizer, J., 2012. Coarse head pose estimation of construction equipment operators to formulate dynamic blind spots. *Advanced Engineering Informatics* 26 (1), 117–130.
- Ray, S.J., Teizer, J., 2012. Real-time construction worker posture analysis for ergonomics training. *Advanced Engineering Informatics* 26, 439–455.
- Ray, S.J., Teizer, J., 2013. Computing blind spots of construction equipment: implementation and evaluation of an automated measurement and visualization method. *Automation in Construction* (in press).
- Teizer, J., Allread, B.S., Mantripragada, U., 2010. Automating the blind spot measurement of construction equipment. *Automation in Construction* 19, 491–501.
- Teizer, J., Allread, B.S., Fullerton, C.E., Hinze, J., 2010. Autonomous pro-active real-time construction worker and equipment operator proximity safety alert system. *Automation in Construction* 19 (5), 630–640.

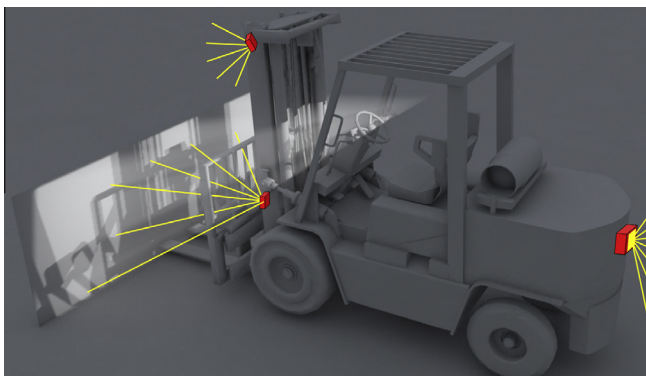


Fig. 30. CAD model produced from scanning and the concept of using the model to show where 3D imagers (red boxes with yellow imaging rays) could be mounted to capture non-visible regions (for a forklift without payload). (For interpretation of the references to colour in this figure legend, the reader is referred to the web version of this article.)